JOURNAL OF THERMOPHYSICS AND HEAT TRANSFER
Vol. 21, No. 2, April–June 2007

Thermohydraulic Modeling of Capillary Pumped Loop and Loop Heat Pipe

Abhijit A. Adoni,* Amrit Ambirajan,† V. S. Jasvanth,† and D. Kumar†
ISRO Satellite Centre, Bangalore 560 017, India
and
Pradip Dutta‡ and K. Srinivasan§
Indian Institute of Science, Bangalore 560 012, India

DOI: 10.2514/1.26222

Capillary pumped loop (CPL) and loop heat pipe (LHP) are passive heat transport devices that are gaining importance as a part of the thermal control system of modern high power spacecraft. A mathematical model to simulate the thermohydraulic performance of CPLs and LHPs is required for the design of such a thermal control system. In this study a unified mathematical model to estimate thermal and hydraulic performance of a CPL and an LHP with a two-phase or a hard-filled reservoir is presented. The steady-state model is based on conservation of energy and mass in the system. Heat exchange between the loop and the surroundings and pressure drops in the loop are calculated. This study presents the results of numerical studies on a CPL and an LHP. The constant conductance regime in a CPL or an LHP occurs when the reservoir is hard-filled. It also occurs in an LHP if the condenser is fully used. The heat leak across the wick becomes significant in a hard-filled LHP because the core is no longer saturated and hence the mass flow rate must be calculated using an energy balance on the outer surface of the wick.

Nomenclature

A	=	area (generally flow area), m^2
C	=	specific heat, $J \cdot kg^{-1} \cdot K^{-1}$
D	=	diameter, m
F_{LHP}	=	energy imbalance in the evaporator core and CC, W
f	=	Darcy friction factor
G	=	mass velocity, $kg \cdot m^{-2} \cdot s^{-1}$
H	=	heat transfer coefficient, $W \cdot m^{-2} \cdot K^{-1}$
h	=	enthalpy, $J \cdot kg^{-1}$
K	=	wick permeability, m^2
k	=	thermal conductivity, $W \cdot m^{-1} \cdot K^{-1}$
L	=	length, m
L_{cond}	=	length of condenser, m
$L_{condensation}$	=	length of condensation, m
$L_{evap\text{-}rt}$	=	distance between points 7 and 4, m
$L_{rt\text{-}hydr}$	=	vertical distance between loop and the reservoir, m
L_{step}	=	refers to step size in RKM, m
M	=	mass of working fluid, kg
$\dot{m}$	=	mass flow rate, $kg \cdot s^{-1}$
P	=	pressure, Pa
Q	=	heat, W
$Q_{deprime}$	=	heat load at which CPL deprimes for limited condenser length, W
Q_{hf}	=	heat load at which reservoir is hard-filled, W
Q_{open}	=	heat load at which condenser fully opens, W
r	=	radius, m
T	=	temperature, K
t	=	thickness, m
U	=	overall heat transfer coefficient, $W \cdot m^{-2} \cdot K^{-1}$
u	=	velocity, $m \cdot s^{-1}$
V	=	volume, m^3
x	=	dryness fraction of vapor
z	=	length, m
α_v	=	void fraction, A_v/A
β	=	volume fraction of liquid in the reservoir
Γ	=	perimeter, m
ϵ	=	porosity
ε	=	numerical error (convergence criterion)
ϑ	=	normalized energy imbalance
λ	=	conductance, $W \cdot K^{-1}$
ρ	=	density, $kg \cdot m^{-3}$
σ	=	surface tension, $N \cdot m^{-1}$
ϕ	=	two-phase friction multiplier

Subscripts

acc	=	acceleration
c	=	core
cond	=	condenser
cond′	=	refers to region where condensation is occurring
e	=	effective
evap	=	evaporator
ex	=	exchange
f	=	friction
fg	=	difference in thermodynamic property in liquid and vapor phase
g	=	groove
i	=	inner part of tube
ins	=	insulation
L	=	leak
l	=	liquid
ll	=	liquid line
lo	=	liquid only
load	=	refers to heat load applied externally
loop	=	part of the system excluding the reservoir
o	=	outer part of tube
P	=	pressure
r	=	reservoir/radial
res	=	reservoir
sc	=	subcooler
sink	=	sink of condenser
t	=	tube/evaporator teeth

Received 28 June 2006; revision received 6 September 2006; accepted for publication 1 October 2006.

*Engineer, Thermal Systems Group; abhijit@isac.gov.in.
†Engineer, Thermal Systems Group.
‡Associate Professor, Department of Mechanical Engineering.
§Formerly Professor, Department of Mechanical Engineering.

tp	=	two-phase
v	=	vapor/(volume in case of specific heat)
vl	=	vapor line
vo	=	vapor only
w	=	wick
wp	=	wick pore
ws	=	particle diameter in sintering
z	=	length direction
ω	=	wall of tube
∞	=	ambient

I. Introduction

CAPILLARY pumped loops (CPL) and the closely related loop heat pipes (LHP) are two-phase heat transport devices that rely on surface tension force induced by a fine pore wick to drive a working fluid in a loop. These are based on a working principle similar to heat pipes: closed evaporation and condensation cycle being maintained by capillary pumping. The principal feature that distinguishes CPLs (and LHPs) from heat pipes is that they do not have a distributed wicking structure. Figure 1 shows schematics of a CPL and an LHP. The vapor and the liquid lines are smooth-walled tubes, with the porous structure limited to the evaporator, which results in lower pressure drop and allows use of a fine pore size (in evaporator), yielding high capillary pressure. An important component of the CPL is the two-phase reservoir, which is plumbed into the liquid line and allows some controllability of loop temperatures. Operating principle of CPLs and LHPs is explained in [1–4]. In a three-port CPL, the reservoir is directly plumbed into the core of the evaporator. The LHP is a variant of the CPL, with the reservoir alongside the evaporator (Fig. 1). The reservoir of a LHP is often referred to as a compensation chamber (CC) in the literature. In this paper these terms are used interchangeably. A secondary wick is often used to ensure that the primary wick is always saturated with liquid, and also to provide a good thermal link between the reservoir and the core. A bayonet is often provided in the evaporator [2,4,5]. In general capillary evaporators can be either *flat plate* (FP) or *tubular axially grooved* (TAG). The principal difference between these evaporators is the shape of the wick; the vapor grooves can either be on the casing or on the wick.

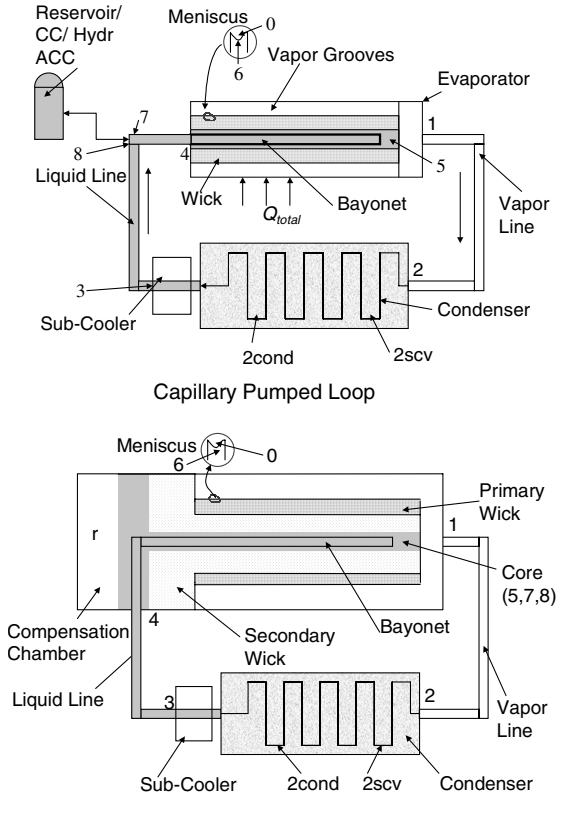

Fig. 1 Schematic of a CPL and LHP.

A situation termed *hard-fill* arises in CPLs and LHPs. For large mass of charge and high heat loads the reservoir is completely full of subcooled liquid. This may also occur in LHP system with multiple evaporators [3] where all the compensation chambers, except the one that is controlling the operating temperature of the loop, are hard-filled. The relationship between the heat load and the evaporator temperature is approximately linear (constant conductance mode) in a hard-filled LHP [4] and CPL [1,6]. Linear behavior, in LHPs, is also observed when the fluid leaving the condenser is neither completely saturated nor subcooled; vapor has not completely condensed in the condenser, i.e., the length of condenser is not sufficient to completely condense the vapor. Under *non-hard-filled* conditions, the essential difference is that the reservoir (in a CPL) and compensation chamber (in a LHP) have saturated fluid, i.e., two phases exist. The core in the LHP has good thermal and hydraulic coupling with the CC, and is almost an extension of CC. The core in a CPL is generally subcooled over most of its operating range; however, it is possible to have a superheated core [7].

CPLs were invented in the United States in the 1960s [8] and the LHPs were independently developed in Russia in the 1970s [9]. Active development of CPLs and LHPs began in the late 1970s. Over the years, this technology has advanced very rapidly. Several ground tests and flight experiments have verified CPL operational characteristics. Ku [2,3] and Maidanik [4] give a brief chronology of developments in CPLs and LHPs, review advances in CPL/LHP technology, and provide numerous applications.

CPL/LHP technology has made significant advances over the years with applications from cryogenic temperatures to moderate temperatures [2–4], with varying evaporator designs and wick material [2–4,10–14] and several working fluids [3,4]. High temperature LHPs have also been designed [4]. Theoretical treatment of the thermohydraulics of CPLs and LHPs has also been undertaken by several researchers. Schweikart and Neiswanger [15] developed an analytical modeler for modeling CPL thermohydraulics, which was experimentally verified. Wulz and Embacher [13] presented a steady-state model using PHOENICS. Dickey and Peterson [16] compared steady-state and transient model of an LHP with experimental data. They also modeled the adverse tilt effects. Murakoa et al. [10,11] theoretically and experimentally studied an LHP with a porous element in the condenser under steady-state and transient conditions. They adopted a nodal transient model to estimate temperatures. They define various regimes (or limits of operation) of operation and model the process of bubble formation in the compensation chamber. Kiper et al. [12] have presented a transient model of a CPL with flat evaporator. Parker [17] developed steady-state and transient LHP model using SINDA/FLUINT.

Kaya and Hoang [18] presented a mathematical model for steady-state thermohydraulic performance of an LHP. The solution procedure involves estimation of conduction heat leak through the wick. The temperature drop across the wick is evaluated using the Clausius–Clapeyron relation. Heat transfer and pressure drop in the vapor line, condenser, subcooler, and liquid line are modeled. LHP operating temperature is determined by solving the energy balance equation. This model can simulate both the constant conductance (fully open condenser) and variable conductance (partially open condenser) operating regimes of an LHP with two-phase compensation chamber. Chuang [19] extended the previous model to analyze the tilt effects on steady-state performance and experimentally validated this.

These previous theoretical and experimental studies have significantly improved understanding of mathematical modeling of CPLs and LHPs with two-phase reservoirs. The authors have not come across mathematical models, in open literature, that deal with the operational characteristics of CPL and LHP systems with hard-filled reservoirs. CPL and LHP systems are not generally designed for hard-filled reservoir under normal operating conditions. However, Maidanik [4] mentions that in many LHPs the linear regime occurs with a hard-filled reservoir. Knowledge of their

performance with hard-filled reservoir would thus be useful in deciding design margins.

In this study, a steady-state thermohydraulic model for CPLs and LHPs is presented that also accounts for situations wherein the reservoir (or compensation chamber) is hard-filled. The differences in the modeling and operational characteristics of CPLs and LHPs are also explained.

II. CPL and LHP Mathematical Model Formulation

The goal of the mathematical model of the CPL/LHP is to determine the operating temperatures and pressures at various locations in the loop as a function of input power. The specified conditions include temperature of the sink, ambient temperature, mass of charge (working fluid), physical dimensions of various components, and thermophysical properties of the working fluid used in the CPL/LHP. This section will outline the mathematical formulation for evaluating the temperatures and pressures at the state points shown in Fig. 1. A description of these state points is tabulated in Table 1.

Circulation of working fluid in the loop is possible only if the total loop pressure drop does not exceed the maximum possible capillary pressure (capillary limit) permissible across the meniscus located at the liquid–vapor interface in the wick. This is expressed by the inequality

$$\Delta P_{c\max} \geq P_1 - P_6 = \Delta P_{12} + \Delta P_{23} + \Delta P_{34} + \Delta P_{56} \qquad (1)$$

where the maximum capillary pressure ($\Delta P_{c\max}$) is given by the Laplace–Young equation $\Delta P_{c\max} = 2\sigma\cos(\theta)/r_{\text{wp}}$, r_{wp} is the pore radius of the wick, and θ is contact angle. Other possible limits in CPLs and LHPs have been outlined by Faghri [20] and Chuang [19].

Assumptions involved in the development of the CPL and LHP thermohydraulic mathematical model are as follows: 1) heat and mass transfer in the wick are only in the radial direction; 2) wick is fully saturated with liquid; 3) the sink temperature (coolant temperature) is assumed to be constant, and the heat transfer coefficient between the outer wall of the tube and sink is constant along the length; 4) fluid flow in the loop is 1-D; 5) the fluid flow in the vapor line and liquid line is assumed to be fully thermally and hydraulically developed; 6) pressure P_4 at the inlet of the evaporator and that in the core P_5 are same; 7) there is negligible pressure drop in the vapor grooves of the evaporator; 8) vapor leaving the evaporator is saturated; 9) negligible viscous dissipation; and 10) in an LHP, the thermodynamic state of the core and compensation chamber are identical.

In the following subsections, mass, momentum, and energy conservation equations are developed for all components of a CPL or an LHP system: namely, evaporator, liquid line, vapor line, condenser, and reservoir. Equations are presented for both FP and TAG evaporators. Wherever relevant, the distinction between CPL and LHP modeling procedure is described. A C-language simulation program was written to iteratively solve the resulting system of nonlinear algebraic and ordinary differential equations. Subsequent sections will outline the algorithms used in this program followed by discussion of results of a case study. Thermophysical properties of the working fluids are obtained using NIST—REFPROP:7.0 FORTRAN source codes (produced by National Institute of Standards and Technology). These FORTRAN source codes were integrated into the simulation program.

Table 1 State points and descriptions

State point	Description
0	Just above the meniscus
1	Exit of evaporator; referred to in this note as evaporator.
2	Exit of vapor line/entry of condenser. Vapor may be superheated.
2scv	Saturated vapor (end of sensible cooling of vapor in condenser)
2cond	Saturated liquid (point at which condensation is finished in condenser)
3	Exit of condenser/entry to liquid line
4	Exit of liquid line/entry to evaporator
5	Core of evaporator wick
6	Point just below the meniscus (liquid side)
7	Location on liquid line immediately after the point where the reservoir is plumbed
8	Location on liquid line immediately before the point where the reservoir is plumbed
r	Reservoir

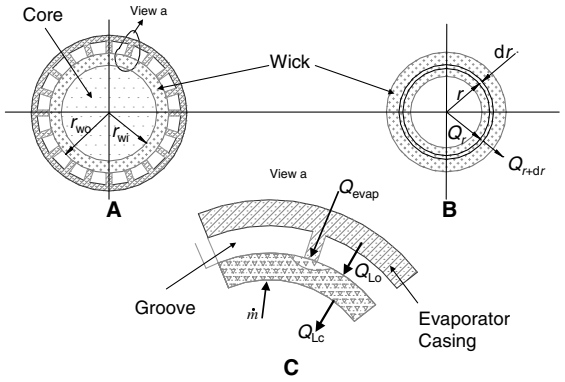

Fig. 2 Schematic of a TAG evaporator. a) Sectional view of TAG evaporator, b) section of evaporator wick, c) energy balance in the evaporator grooves.

A. Thermohydraulics of the Evaporator

Figure 2 illustrates the heat transfer processes occurring in the evaporator. Of the total heat load (Q_{load}) supplied to the evaporator, a part is conducted radially inward through the outer surface of the wick (Q_{evap}) and the balance is convected to the surroundings and also possibly conducted to the reservoir or compensation chamber. The evaporator *casing* temperature is estimated by

$$T_{\text{evap}} = T_0 + \frac{Q_{\text{evap}}}{H_{\text{evap}} A_t} \qquad (2)$$

where H_{evap} is the heat transfer coefficient between the casing and the outer surface of the liquid saturated wick and A_t is the contact area between the evaporator casing and the wick. It is assumed that the sensible heating in the evaporator grooves is negligibly small compared to Q_{evap}, as evaporation heat transfer coefficient at the wick and evaporator casing interface is extremely large compared to that in the grooves. The phenomena in this region are complex and the value of this parameter (H_{evap}) may be deduced experimentally. T_0 is the fluid temperature of the wick at the tooth-wick interface; state points 0 and 1 are to be assumed identical. Based on an energy balance in the evaporator, Q_{evap} is given by

$$Q_{\text{evap}} = Q_{\text{load}} - \underbrace{Q_{\text{evap-}r}}_{\text{to reservoir}} - \underbrace{H_{\text{evap-}\infty} A_{\text{evap-ins}} (T_{\text{evap}} - T_\infty)}_{\text{to ambient}} \qquad (3)$$

Note that $Q_{\text{evap-}r} = Q_{\text{Lr}}$ if the reservoir is plumbed/welded to the evaporator; otherwise $Q_{\text{evap-}r} = 0$. A procedure to evaluate Q_{Lr} in a CPL and LHP is explained later in this section. For most terrestrial LHP tests, the evaporator is insulated. Thus heat loss to the ambient will be a small fraction of Q_{load}. The heat transmitted through the teeth (Q_{evap}) is used to heat the subcooled liquid in the wick (Q_{Lo}) and vaporize the liquid at the liquid-vapor interface in the wick; hence an energy balance on the outer surface of the evaporator wick (Fig. 2) is given by

$$Q_{\text{evap}} = \underbrace{\dot{m} h_{\text{fg},1}}_{\text{vaporization}} + Q_{\text{Lo}} \qquad (4)$$

$\dot{m}$ is iteratively evaluated for given T_1 and T_5 using thermophysical properties evaluated at states 1 and 5, respectively. It should be noted

that the leak on the outer surface is considered in estimating $\dot{m}$, as it is significant compared to Q_{evap} in a CPL and hard-filled LHP.

The pressure at P_6 is lower than the core pressure (P_5) due to the Darcian pressure drop in the wick (ΔP_w) and is given by

$$P_6 = P_5 - \Delta P_w \tag{5}$$

It should be noted that T_6 and T_0 are assumed identical to T_1. The mass of working fluid (MWF) in the evaporator is obtained by adding the mass of liquid in the core and wick to the mass of vapor in the vapor grooves:

$$M_{\text{evap}} = \rho_5 V_c + \rho_{v,1} V_g + \rho_5 \epsilon V_w \tag{6}$$

Methods for evaluation of Q_{Lo} and Q_{Lc} in a TAG and FP evaporator are explained next, followed by methodologies for evaluating the thermodynamic state of the core in a CPL and LHP, respectively.

1. Heat Transfer and Pressure Drop in the Evaporator Wick

In a TAG evaporator wick, the local temperature is dictated by an energy balance between the radially *outward* flowing liquid and the radially *inward* conducted heat ($-Q_r$). Thus, the energy equation in the porous liquid saturated wick, assuming local identical liquid and wick temperatures, is

$$2\pi k_{\text{we}} L_w \frac{\mathrm{d}}{\mathrm{d}r}\left(r\frac{\mathrm{d}T}{\mathrm{d}r}\right) = \dot{m} C_{p15}\frac{\mathrm{d}T}{\mathrm{d}r} \tag{7}$$

where C_{p15} is the mean specific heat of the working fluid between 1 and 5, k_{we} is the effective thermal conductivity of the wick accounting for conduction through the solid and liquid, and L_w is the length of the wick. There are several models for evaluation of thermal conductivity of wicks saturated with liquid [21]. Here, effective thermal conductivity of the wick is calculated using $k_{\text{we}} = \epsilon k_l + (1-\epsilon)k_w$. Solving the energy equation [Eq. (7)] using the boundary conditions $T|_{r=r_i} = T_5$ and $T|_{r=r_o} = T_1$, the heat leaks on the outer (Q_{Lo}) and inner surface (Q_{Lc}) of the TAG wick [22] are given by

$$Q_{\text{Lo}} = -Q_r|_{r=r_o} = \frac{\dot{m} C_{p15}}{1-\gamma}(T_1 - T_5) \tag{8}$$

$$Q_{\text{Lc}} = -Q_r|_{r=r_i} = \gamma * Q_{\text{Lo}} \tag{9}$$

where

$$\gamma \equiv (D_{\text{wi}}/D_{\text{wo}})^{\dot{m}C_{p15}/2\pi k_{\text{we}} L_w} \tag{10}$$

Pressure drop in the wick is evaluated using the Darcy relation for pressure drops in a cylindrical porous medium [20]:

$$\Delta P_w = \frac{\mu_{15}}{K}\frac{\dot{m}}{2\pi L_w \rho_{15}}\ell_n \frac{D_{\text{wo}}}{D_{\text{wi}}} \tag{11}$$

where μ_{15} and ρ_{15} are, respectively, the average viscosity and average density between states 1 and 5. Permeability for a sintered metal wick is evaluated using the Blake–Cozeny equation [23] $K = D_{\text{ws}}^2\epsilon^3/[37.5(1-\epsilon)^2]$, where D_{ws} and ϵ are the particle diameter used for sintering the medium and porosity, respectively.

Similarly, for the wick in a flat plate evaporator, Q_{Lo} and Q_{Lc} are given by

$$Q_{\text{Lo}} = -Q_z|_{z=0} = \frac{\dot{m} C_{p15}\gamma'}{\gamma' - 1}(T_1 - T_5) \tag{12}$$

$$Q_{\text{Lc}} = -Q_z|_{z=t_w} = Q_{\text{Lo}}/\gamma' \tag{13}$$

where $\gamma' \equiv \exp[\dot{m}C_{p15}t_w/(k_{\text{we}}A_w)]$. In case of FP evaporators, the core is additionally heated through the evaporator casing. If $\lambda_{e,\text{evap-}c}$ is the effective thermal conductance between the evaporator casing and the liquid core, the leakage is evaluated by $Q_{\text{evap-}c} = \lambda_{e,\text{evap-}c}(T_{\text{evap}} - T_5)$. This leakage requires that the expression for Q_{evap} [Eq. (3)] be modified for FP evaporators to

$$Q_{\text{evap}} = Q_{\text{load}} - Q_{\text{evap-}r} - H_{\text{evap-}\infty}A_{\text{evap-ins}}(T_{\text{evap}} - T_\infty) - Q_{\text{evap-}c} \tag{14}$$

Analogous to Eq. (11), the pressure drop in the wick for flat plate evaporator is

$$\Delta P_w = \frac{\mu_{15}}{K}\frac{\dot{m}}{\rho_{15}A_w} \tag{15}$$

2. Modeling of Heat Transfer in Reservoir Tube

In a CPL, the reservoir may be plumbed either to the liquid line or the evaporator [24]. The heat leak to the reservoir, Q_{Lr}, is important in determining the temperature of the evaporator. In this section heat transfer in the insulated tube connecting the loop with the reservoir is modeled as a one-dimensional convecting fin. Solving the fin equation ($\mathrm{d}^2\theta/\mathrm{d}z^2 = \chi^2\theta$) and related boundary conditions ($\theta|_{z=0} = \theta_8, \theta|_{z=L_{rt}} = \theta_r$) yields

$$Q_{\text{Lr}} = -A_{e,\text{rt}}k_{e,\text{rt}}\left.\frac{\mathrm{d}\theta}{\mathrm{d}z}\right|_{z=0} = -k_{e,\text{rt}}A_{e,\text{rt}}\chi\frac{\theta_r - \theta_8\cosh(\chi L_r)}{\sinh(\chi L_{\text{rt}})} \tag{16}$$

where $\theta \equiv T - T_\infty$, $H_{\text{rt,ins-}\infty}$ is heat transfer coefficient of insulation with surroundings, $\Gamma_{\text{rt,ins}}$ is perimeter of tube insulation and $\chi^2 \equiv (H_{\text{rt,ins-}\infty}\Gamma_{\text{rt,ins}})/(k_{e,\text{rt}}A_{e,\text{rt}})$. Note that $k_{e,\text{rt}}$ is the area weighted thermal conductivity of the tube based on insulation, tube wall, and fluid. $A_{e,\text{rt}}$ is the total cross section area of the tube including the insulation. In a CPL, if the reservoir tube is plumbed to the evaporator casing (three-port configuration) then θ_8 is replaced by θ_{evap}. For an LHP, due to the proximity of the compensation chamber with respect to the evaporator, Q_{Lr} is given by $Q_{\text{Lr}} = \lambda_{\text{evap-}r}(T_{\text{evap}} - T_r)$, where $\lambda_{\text{evap-}r} = k_{\text{rt}}A_{\text{rt}}/L_{\text{rt}}$ is thermal conductance between the evaporator and reservoir.

3. Evaluation of Thermodynamic State of the Core in a CPL

The core of the evaporator of a CPL has the same pressure as that of the liquid line exit (assumption 6). Thus the momentum equation and the energy balance equation are

$$P_5(T_5, \rho_5) = P_4 \tag{17}$$

$$Q_{\text{Lc}}(T_5) = \dot{m}C_{p54}(T_5 - T_4) \tag{18}$$

In an FP evaporator $Q_{\text{evap-}c}$ is added to the left-hand side of Eq. (18) to account for additional leak to the core from the evaporator casing. Equations (17) and (18) are solved simultaneously for T_5 and ρ_5, assuming T_1 and $\dot{m}$ are constant.

4. Evaluation of Thermodynamic State of the Core in an LHP

In LHPs, the core is assumed to be saturated until it is hard-filled. The bayonet is not considered, and the liquid from the liquid line enters the reservoir. Hence (when the core is saturated),

$$P_5 = P_4 \tag{19}$$

$$T_5 = T_{\text{sat}}(P_5) \tag{20}$$

where $T_{\text{sat}}(P_5)$ is the saturation temperature corresponding to pressure P_5. Energy balance equation for an LHP core is

$$Q_{\text{Lc}} + Q_{\text{Lr}} + x_4\dot{m}h_{fg5} = A_r U_{r\text{-}\infty}(T_r - T_\infty) + \dot{m}C_{p54}(T_5 - T_4) \tag{21}$$

where Q_{Lc} and Q_{Lr} are evaluated based on the procedure outlined earlier in this section. The third term on the left is the latent heat that

needs to be rejected when the fluid entering the core has some vapor in it. The first term on the right-hand side accounts for the heat exchange between the reservoir and the ambient ($Q_{r\text{-}\infty}$) and the second term on the right represents the sensible heating of the liquid entering the core. Equation (21) is solved iteratively for T_1. The difference in evaluation of thermodynamic state of the core, and subsequently state of point 1 in the loop, is the major distinction in modeling of an LHP and a CPL.

For LHPs with *hard-filled reservoir* (reservoir has subcooled liquid) the equation of state [Eq. (19)] and energy balance in the core [Eq. (21)] are solved simultaneously for T_5 and ρ_5. For an LHP, by virtue of assumption 10, $T_r \sim T_5$. Also state points 5, 7, and 8 are identical as the reservoir is directly plumbed to the core.

B. Single Phase Flow

This section describes the procedure to calculate pressure drop, heat exchange, and MWF for single phase flow in a tube, as occurs in the vapor line, liquid line, and subcooler section of the condenser. The relevant ODEs have the form

$$\frac{\mathrm{d}T_t}{\mathrm{d}z} = -\frac{U_{t-\infty}\Gamma_t(T_t - T_\infty)}{\dot{m}C_{p,t}} \tag{22}$$

$$\frac{\mathrm{d}P_t}{\mathrm{d}z} = -f\frac{G^2}{2\rho_t D} \tag{23}$$

$$\frac{\mathrm{d}M_t}{\mathrm{d}z} = A_t\rho_t \tag{24}$$

where the subscript t represents either vapor line (vl), liquid line (ll), or subcooler (sc). $U_{t\text{-}\infty}$ is the overall heat transfer coefficient between the fluid and the ambient. $U_{t\text{-}\infty}$ is chiefly dictated by the heat transfer coefficient between the outer tube wall (or the tube insulation) and the ambient ($H_{t\text{-}\infty}$) and is assumed to be constant here. The heat transfer coefficient between the fluid and the tube wall can be calculated using correlations as presented in [25]. When modeling the subcooler, the subscript ∞ should be replaced by *sink*. Equation (24) indicates the mass distribution of working fluid in the tube.

A sixth-order Runge–Kutta method (RKM) [26] is used for solving the ODEs. Initial conditions are defined at the inlet of the tube. Thermophysical properties are calculated at the beginning of each length step. If phase change occurs in the liquid line (boiling) or vapor line (condensation) the fluid is treated as saturated [with the fluid properties of saturated vapor (vapor line) or saturated liquid (liquid line)] for evaluation of heat transfer, pressure drops, and MWF in the tube. The fluid is at the saturation temperature corresponding to the pressure at the end of each length step in RKM. Exit quality at the end of each length step is obtained based on an energy exchange during the length step.

C. Condenser

This section outlines the method to evaluate heat transfer, pressure drop, and mass of condensing fluid in the condensing section of the loop: namely, condenser and liquid line (if $x_3 > 0$). At point 2 the vapor is either saturated or the degree of superheat is small, hence the length of condenser tube required to cool the vapor to saturation is extremely small. Therefore, the pressure at state 2scv is assumed to be the same as that at state 2 and the vapor is saturated. The temperature at state 2scv corresponds to the saturation temperature at $P_{2\mathrm{scv}}$. Condensation starts at point 2scv and completes at point 2cond. $L_{\mathrm{condensation}}$ is the distance between points 2scv and 2cond, i.e., the length of condenser required to completely condense saturated vapor from state 2scv. In an LHP, it is possible that at high heat loads vapor may not completely condense in the condenser, resulting in nonzero exit quality.

The overall heat transfer coefficient based on inner diameter of the tubing between the condensing fluid and the sink is given by

$$\frac{1}{U_{\mathrm{cond}'}} = \frac{D_{\mathrm{cond},i}}{2k_{\mathrm{cond},t}}\ell_n\left(\frac{D_{\mathrm{cond},o}}{D_{\mathrm{cond},i}}\right) + \frac{D_{\mathrm{cond},i}}{D_{\mathrm{cond},o}H_{\mathrm{sink}}} + \frac{1}{H_{\mathrm{cond}'}} \tag{25}$$

Energy balance for an infinitesimal length of condenser and pressure gradient in the condenser during condensation (neglecting gravitational effects) [27] are given by

$$\frac{\mathrm{d}x_{\mathrm{cond}'}}{\mathrm{d}z} = -\frac{U_{\mathrm{cond}'}(T_{\mathrm{cond}'} - T_{\mathrm{sink}})\pi D_{\mathrm{cond},i}}{\dot{m}h_{\mathrm{fg}}} \tag{26}$$

$$\frac{\mathrm{d}P_{\mathrm{cond}'}}{\mathrm{d}z} = \underbrace{-\phi_{\mathrm{lo}}^2\frac{fG^2}{2\rho_{\mathrm{lo}}D_{\mathrm{cond},i}}}_{\text{frictional}} \underbrace{- G^2\frac{\mathrm{d}}{\mathrm{d}z}\left\{\frac{(1-x_{\mathrm{cond}'})^2}{\rho_l(1-\alpha_v)} + \frac{x_{\mathrm{cond}'}^2}{\rho_v\alpha_v}\right\}}_{\text{acceleration}} \tag{27}$$

MWF variation at any point during condensation is given by

$$\mathrm{d}M_{\mathrm{cond}'}/\mathrm{d}z = A_{\mathrm{cond}}[\alpha_v\rho_v + (1-\alpha_v)\rho_l] \tag{28}$$

One way to solve the preceding ODEs is to numerically integrate Eqs. (26–28), assuming constant thermophysical properties during condensation [18]. In this study the preceding ODEs [Eqs. (26–28)] are solved simultaneously using the RKM to obtain $P_{2\mathrm{cond}}$ and mass of condensing fluid in the condenser ($M_{\mathrm{cond}'}$). $x_{2\mathrm{cond}}$ and $L_{\mathrm{condensation}}$ are also evaluated. Note that thermophysical properties are evaluated at *every* length step. The initial conditions for the ODEs [Eqs. (26–28)] are $x_{\mathrm{cond},0} = x_{2\mathrm{scv}}$, $P_{\mathrm{cond},0} = P_{2\mathrm{scv}}$, and $M_{\mathrm{cond}',0} = 0$.

Several correlations are available in literature for estimating $H_{\mathrm{cond}'}$, ϕ_{lo}, and α_v. In this paper regime based correlations proposed by Thome et al. [28,29] are used for evaluation of $H_{\mathrm{cond}'}$ and α_v. These correlations need the inner wall temperature of the condenser tube given by $T_\omega = T_{\mathrm{sink}} - \dot{m}h_{fg}\Delta x_{\mathrm{cond}'}/(H_O\Gamma_{\mathrm{cond},i}L_{\mathrm{step}})$. ϕ_{lo} is evaluated using Friedel correlation [25]. Finally, the MWF in the condenser is calculated by

$$M_{\mathrm{cond}} = M_{\mathrm{cond}'} + M_{\mathrm{sc}} \tag{29}$$

The procedure for calculating M_{sc} is given in Sec. II.B.

III. Numerical Scheme

The numerical scheme adopted here is a variant of the fixed point iteration technique [26] for a nonlinear system of equations, and is used to predict temperature, pressure, and mass distribution in the loop. Newton–Raphson method (NRM) is used to minimize energy balance residue, pressure imbalance, and mass imbalance. There are ODEs to be solved for some components, viz. vapor line, liquid line, and the condenser. Upon solving the ODEs the thermodynamic state at the exit of the component is obtained. The fixed point iteration scheme adopted here involves sequential solving of these equations, namely, ODE or nonlinear equations as discussed in Sec. II, along the loop for each component. This approach is explained in detail through algorithms A0, A1-CPL, A1-LHP, and A2. The primary algorithm A2, is applicable to LHPs and CPLs for saturated *and* hard-filled reservoirs. In the pictorial representation of the algorithms, numerous decision boxes are used. If there is more than one condition in any decision box, then the decision is *yes* only if all conditions are true, unless otherwise stated.

A. Algorithm A0

Algorithm A0 (see Fig. 3) is used to predict temperature, pressure, and MWF in vapor line, condenser, and liquid line, given T_1, T_5, and Q_{load}. The output of this algorithm are the thermodynamic states of the working fluid in the vapor line, condenser, and liquid line.

Q_{evap} is evaluated using Eq. (3) (TAG) or Eq. (14) (FP). T_{evap} is then evaluated using Eq. (2), followed by iteratively solving Eq. (4) for $\dot{m}$. The procedure outlined in Sec. II.C is used to evaluate the heat transfer, pressure drop, MWF, and thermodynamic states of the condensing portion of the condenser. Section II.B describes the methodology to calculate the heat transfer, pressure drop, MWF, and

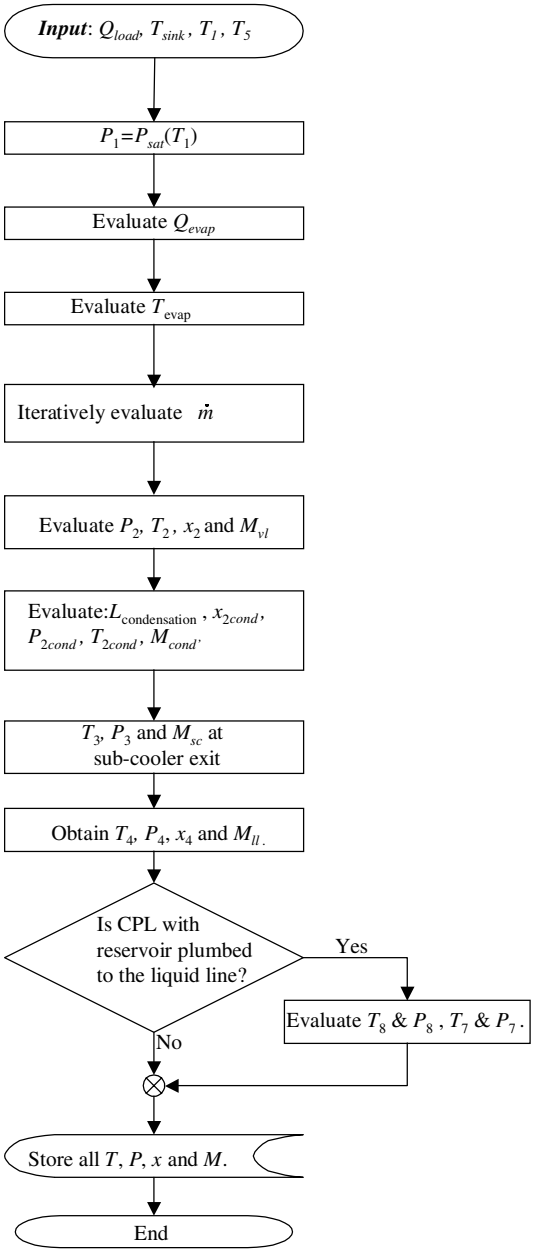

Fig. 3 Algorithm A0 for determination of loop temperatures, $\dot{m}$, and MWF.

thermodynamic state for the vapor line, liquid line, and subcooled portion of the condenser.

B. Algorithm A1-CPL

Algorithm A1-CPL (see Fig. 4) evaluates the temperature, pressure, and mass distribution in different parts of a CPL with a *saturated* reservoir. Inputs to this algorithm are Q_{load}, T_{sink}, T_r, and guess values of T_1 and T_5. This algorithm involves repeated sequential evaluation (fixed point method) of T_5 and ρ_5 [using Eqs. (17) and (18)] until energy and momentum balance is achieved.

First, for a given T_1, temperature at the exit of the liquid line is estimated by calling algorithm A0. Then the thermodynamic state of the core (state point 5) is estimated by solving Eqs. (17) and (18). This procedure is repeated until desired ϑ_{wo} and ϑ_{glob} are reached. ϑ_{wo} and ϑ_{glob} are defined by

$$\vartheta_{\text{wo}} := \left| 1 - \frac{\dot{m} h_{\text{fg},1} + Q_{\text{lo}}}{Q_{\text{evap}}} \right| \tag{30}$$

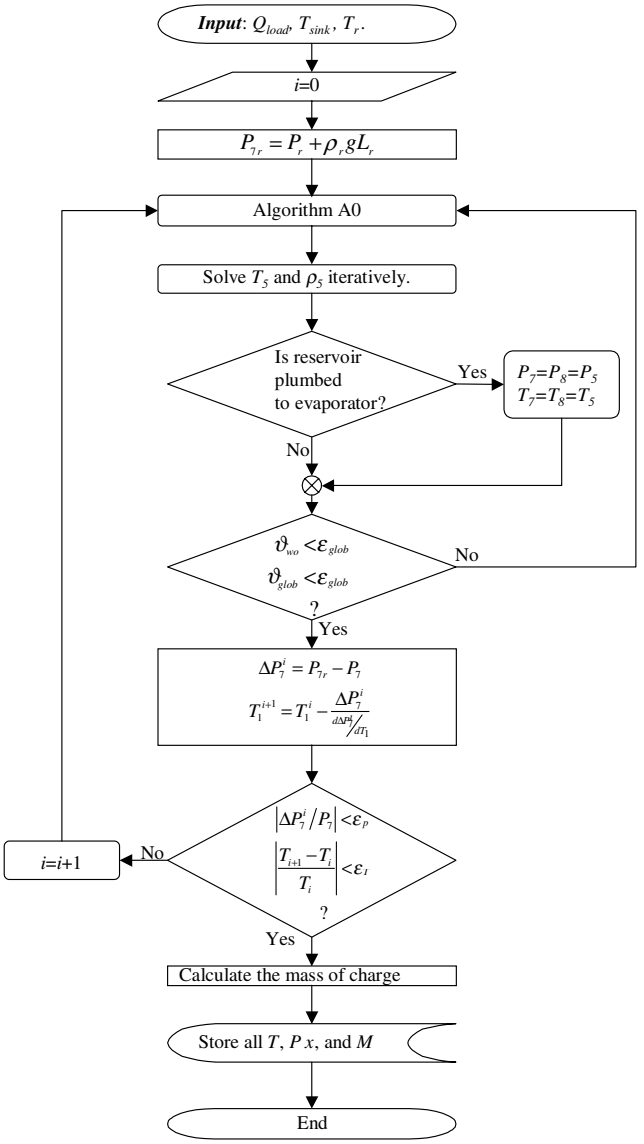

Fig. 4 Algorithm A1-CPL for a CPL with two-phase reservoir.

$$\vartheta_{\text{glob}} := \left| 1 - \frac{Q_{\text{vl}} + Q_{\text{ll}} + Q_{\text{cond}} + Q_{\text{Lr}} + Q_{\text{evap-}\infty}}{Q_{\text{load}}} \right| \tag{31}$$

In the preceding equations, ϑ_{wo} represents the heat balance on the outer surface of the wick normalized with respect to Q_{evap}, and ϑ_{glob} represents global heat balance normalized with respect to Q_{load}.

Now, T_1 is iteratively updated using Newton–Raphson formula until ΔP_7 [defined in Eq. (33)] is minimized. Because the reservoir is assumed to be saturated and the temperature of the reservoir (T_r) is specified, the pressure and density of liquid and vapor in the reservoir are determined. P_{7r}, pressure at point 7, is obtained by adding the hydrostatic head, based on L_{rt}, to the reservoir pressure (P_r).

$$P_{7r} := P_r + \frac{\rho_r + \rho_7}{2} g L_{\text{rt-hydr}} \tag{32}$$

P_7 is obtained from algorithm A0 for reservoir plumbed to the liquid line. If the reservoir is plumbed to the evaporator, as in a three-port CPL, $P_7 = P_8 = P_5$ and $T_7 = T_8 = T_{\text{evap}}$. In this algorithm, the residue ΔP_7, defined as

$$\Delta P_7 := P_{7r} - P_7 \tag{33}$$

Residue, ΔP_7, implies force (or pressure) imbalance at point 7 in the loop. Minimization of ΔP_7 is achieved by iteratively updating T_1 using the Newton–Raphson method. The derivative $\mathrm{d}\Delta P_7/\mathrm{d}T_1$ is

obtained numerically. Every update of T_1 involves evaluation of temperature and pressure based on the procedure outlined earlier in this subsection.

Subsequently MWF in the reservoir (M_r) is obtained by subtracting MWF in loop (M_{loop}) from total mass of charge (M_{tot}).

$$M_r = M_{\text{tot}} - M_{\text{loop}} - M_{rt} \tag{34}$$

where

$$M_{\text{loop}} = M_{\text{vl}} + M_{\text{cond}} + M_{\text{ll}} + M_{\text{evap}} \tag{35}$$

and MWF in the reservoir tube is given by

$$M_{\text{rt}} = V_{\text{rt}}(\rho_7 + \rho_r)/2 \tag{36}$$

The volume fraction of the liquid in the reservoir, β, is obtained from

$$\beta = \left(\frac{M_r}{V_r} - \rho_v\right)/(\rho_l - \rho_v) \tag{37}$$

If the calculated value of β is greater than unity, the reservoir is hard-filled and the CPL is in a constant conductance mode. If this occurs algorithm A2 is used.

C. Algorithm A1-LHP

Algorithm A1-LHP, outlined in Fig. 5, is used for calculation of loop temperature in an LHP with a *saturated* core. Apart from guess values of T_1 and T_5, inputs to this algorithm are Q_{load} and T_{sink}. This algorithm is not applicable to hard-filled reservoir/compensation chamber, hence the core is saturated and its pressure is equal to the liquid line exit pressure (which is obtained from algorithm A0). Equations (19) and (20) are repeatedly evaluated till T_5 converges. The energy equation in the core [Eq. (21)] is solved to evaluate T_1 using Newton–Raphson method. The term F_{LHP}, used in A1-LHP for the T_1 update equation is

$$F_{\text{LHP}}(T_1) := Q_{\text{Lc}} + Q_{Lr} + x_4\dot{m}h_{\text{fg4}} - A_r U_{r-\infty}(T_r - T_\infty) - \dot{m}C_{p54}(T_5 - T_4)$$

F_{LHP} is the energy imbalance in the evaporator core and CC together. The derivative $\mathrm{d}F_{\text{LHP}}/\mathrm{d}T_1$ is obtained numerically. The superscript i of F_{LHP} is the iteration number. In addition to temperature (convergence), convergence is checked for the following heat balance residues to ensure they are less than specified values defined by

$$\vartheta_{\text{wo}} := \left|1 - \frac{\dot{m}h_{\text{fg},1} + Q_{\text{Lo}}}{Q_{\text{evap}}}\right| \tag{38}$$

$$\vartheta_c := \left|\frac{F_{\text{LHP}}}{Q_{\text{Lc}}}\right| \tag{39}$$

$$\vartheta_{\text{glob}} := \left|1 - \frac{Q_{\text{vl}} + Q_{\text{ll}} + Q_{\text{cond}} + Q_{\text{evap-}\infty} + Q_{r-\infty}}{Q_{\text{load}}}\right| \tag{40}$$

The MWF in the CC and volume fraction of liquid in CC are obtained in the same way as explained in the preceding section on A1-CPL [Eqs. (35–37)].

D. Algorithm A2

Algorithm A2, as shown in Fig. 6, is used to predict temperature, pressure, and mass distribution in a CPL or an LHP, given M_{tot}, Q_{load}, and T_{sink}. This is the general algorithm that can handle both saturated and hard-filled reservoir. Initially the reservoir is assumed to be saturated. Mass of charge, system temperature, and pressure are obtained by executing A1-CPL or A1-LHP for a given Q_{load}, T_{sink}, and T_{res} (for CPL). If the calculated value of β is less than 1, then no mass imbalance occurs. However, if $\beta > 1$, mass imbalance exists.

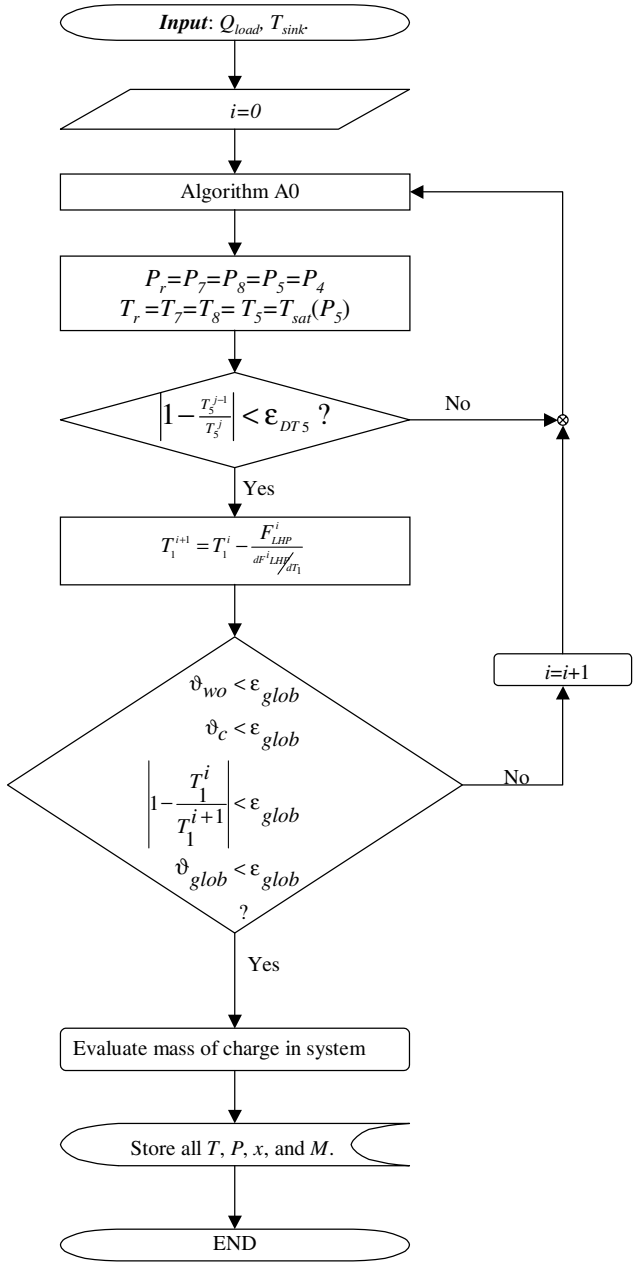

Fig. 5 Algorithm A1-LHP for an LHP with two-phase CC.

Mass imbalance (ΔM) is defined by

$$\Delta M := M_{\text{tot}} - M_{\text{cal}} \tag{41}$$

ΔM is minimized by iteratively updating T_1 using the NRM. The calculated mass of charge (M_{cal}) for hard-filled reservoir is obtained by $M_{\text{cal}} = M_r + M_{\text{rt}} + M_{\text{loop}}$. Evaluation of M_{loop} involves finding of temperatures, pressures, and mass distribution in various components by executing algorithm A0. The thermodynamic state of the core is found by solving Eqs. (17) and (18) in a CPL. In an LHP Eqs. (19) and (21) are solved to determine the state of the core and CC. MWF in the evaporator is then calculated using Eq. (6). MWF in a hard-filled reservoir (M_r) is obtained by $M_r = V_r\rho_r$, where ρ_r is density at T_r and P_r (using equation of state). For a CPL, T_r is specified and $P_r = P_7 - \rho_7 g L_{\text{rt-hydr}}$. In an LHP, $T_r = T_5$ and $P_r = P_5$. M_{rt} is evaluated using Eq. (36). The pressure at state point 6 is evaluated using Eqs. (5) and (11) (for a TAG) or (15) (for a FP). The temperature at state point 6 is same as that at 0. By virtue of assumption 7, state points 0 and 1 are identical.

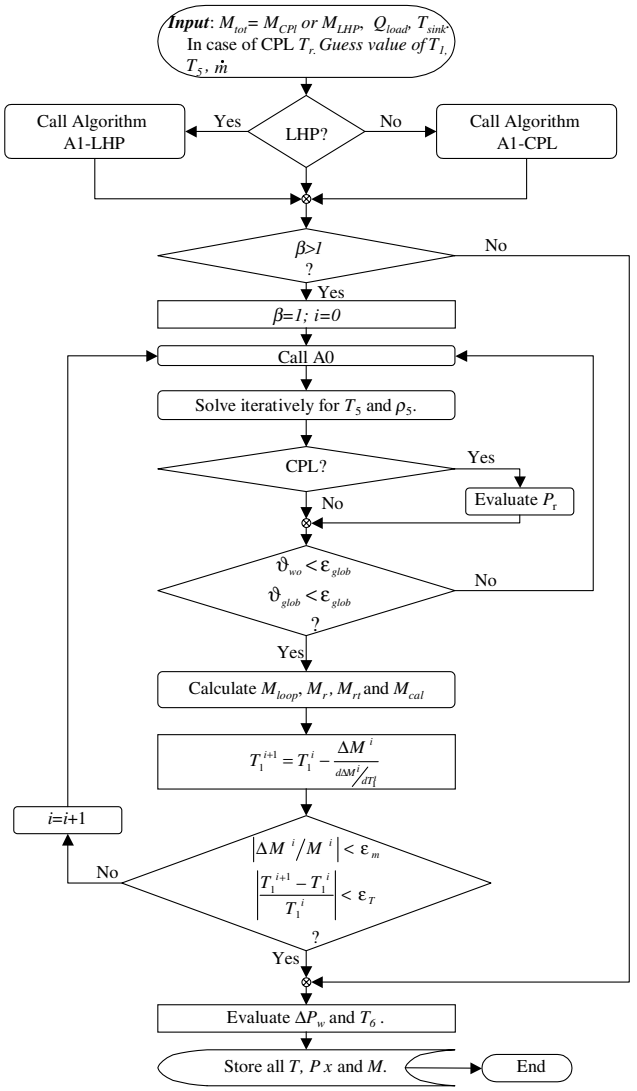

Fig. 6 Algorithm A2 for determination of temperatures, pressure, and mass of charge in a CPL/LHP.

E. Numerical Errors and Experimental Validation

In the algorithms discussed in preceding sections, temperature, pressure, and mass distribution are obtained using fixed point method followed by use of Newton–Raphson method (NRM) to solve energy balance [Eq. (19)] or pressure balance [Eq. (33)] or mass balance [Eq. (41)] equations. The number of iterations required to obtain convergence depends on the guess values. NRM is applied in conjunction with relaxation and bracketing methods (like bisection method) to speed up convergence. All calculations are done with double precision.

For both CPLs and LHPs, the energy balance errors on the wick outer surface and in the core are less than 10^{-5} W and 10^{-3} W, respectively. ϑ_{glob} is less than 1% and temperature convergence is better than 0.01 K. The pressure imbalance at point 7 in a converged solution is less than 1.0 Pa. For the hard-filled LHP and CPL, the mass imbalance (ΔM) in the loop is less than 0.05% of the total mass. The RKM method, which is applied to estimate heat transfer and pressure drop in vapor line, liquid line, and condenser, uses 200 divisions on each component.

During this numerical study, it was observed that global energy balance error in LHPs and CPLs increased with hard-filling. When the reservoir hard-fills, the temperature difference across the wick increases, resulting in significant variation of thermodynamic properties. Preliminary analyses suggest that the variation in specific heat of fluid with temperature must be accounted for when modeling heat transfer in the wick. Inaccuracy in estimation of temperatures can also be introduced due to inaccurate mass flow rate calculations.

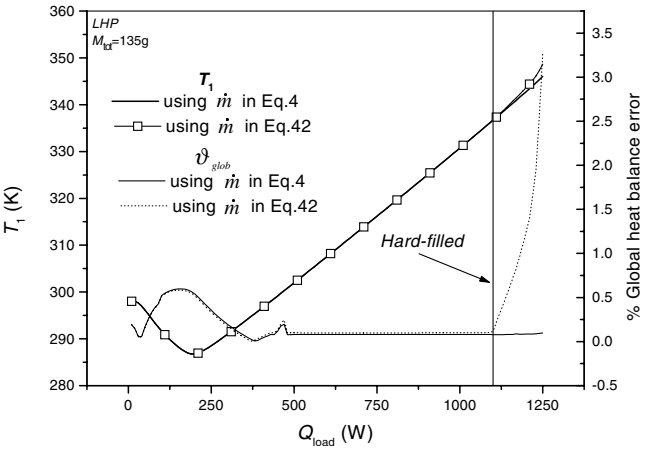

Fig. 7 Effect of $\dot{m}$ on evaluation of evaporator temperature and global heat balance error in an LHP.

If the mass flow rate is estimated by [30,31]

$$\dot{m} \sim Q_{\text{evap}}/h_{\text{fg}} \tag{42}$$

the global energy balance sharply increases upon hard-filling of the reservoir. Figure 7 compares the predicted LHP temperatures, using Eqs. (4) and (42), and normalized global energy balance errors (ϑ_{glob}). It is clear that the heat leak on the wick outer surface plays an important role in estimation of mass flow rate ($\dot{m}$). Use of Eq. (42) in CPLs would introduce large errors in prediction, even with a non-hard-filled reservoir, at moderate heat loads owing to a subcooled core, which results in significant sensible heating of the liquid as it traverses the wick. In this study, Eq. (4) has been used to estimate mass flow rate.

The mathematical model was validated against data obtained from experiments on a three-port CPL with 130 g of acetone as working fluid. The experimental data was obtained with a TAG evaporator connected (in place of the FP evaporator) to the test rig described in [24]. The evaporator details are given in Table 2. The reservoir was directly connected to the core of the evaporator with a 30 mm long, quarter-inch-diameter tube. Experimental and predicted data are plotted in Fig. 8. Because the reservoir is saturated for all heat loads considered here, its temperature is the saturation temperature corresponding to the reservoir absolute pressure. The liquid line and vapor line temperature sensors are located 810 mm and 1300 mm from the evaporator, respectively. The evaporator temperature is the average of six thermocouples. The predicted and experimental data are in good agreement. The discrepancy between predicted and

Table 2 Summary of system parameters

Evaporator wick[a]		Condenser	
L_w	200 mm	L_{cond}	3000 mm
D_{wo}	24.15 mm	$D_{\text{cond},o}$	6.35 mm
D_{wi}	11 mm	$D_{\text{cond},i}$	4.57 mm
H_{evap}	5000 W · m^{-2} · K^{-1}	$H_{\text{cond},o}$	300 W · m^{-2} · K^{-1}
$H_{\text{evap-}\infty}$	0 W · m^{-2} · K^{-1}	$k_{\text{cond},t}$	15 W · m^{-1} · K^{-1}
D_p	10 μm		
k_w	1 W · m^{-1} · K^{-1}		
K	10^{-13} m^2		
Vapor and liquid lines		Reservoir/CC	
L_{vl}	1500 mm	V_r	150 cm^3
L_{ll}	2000 mm	$A_{r,o}$	0.017 m^2
$D_{\text{vl},o}$, $D_{\text{ll},o}$	6.35 mm	T_r	298.15 K
$D_{\text{vl},i}$, $D_{\text{ll},i}$	4.57 mm	L_{rt}	30 mm (for LHP)
$k_{\text{vl},t}$, $k_{\text{ll},t}$	15 W · m^{-1} · K^{-1}	L_{rt}	80 mm (for CPL)
$D_{\text{ins-vl},i}$, $D_{\text{ins-ll},i}$	100 mm	$L_{\text{rt-hydr}}$	80 mm (for CPL)
$k_{\text{ins-vl},t}$, $k_{\text{ins-ll},t}$	0.04 W · m^{-1} · K^{-1}	$L_{\text{evap-rt}}$	500 mm
$H_{\text{vl-}\infty}$, $H_{\text{ll-}\infty}$	10 W · m^{-2} · K^{-1}	$k_{\text{rt},t}$	0.04 W · m^{-1} · K^{-1}
Ambient		Sink	
T_∞	298.15 K	T_{sink}	273.15 K

[a]Evaporator is assumed to have negligible heat transfer with surroundings. LHP does not have a bayonet and liquid directly enters the CC.

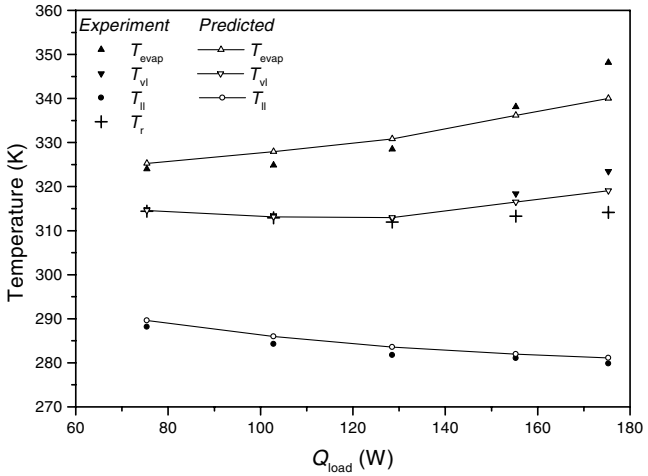

Fig. 8 Experimental and predicted data for a three-port acetone CPL.

observed evaporator temperature is attributed to the use of a constant H_{evap} (675 $W \cdot m^{-2} \cdot K^{-1}$) in the mathematical model. The vapor line is superheated at higher heat loads and is modeled using method analogous to Chuang [19].

IV. Results and Discussion

The algorithms discussed in the preceding section were implemented in a C-language computer program that was run on an SGI-Origin2000 server. Ammonia is the working fluid used in this study. Table 2 gives the details of the of the CPL and LHP used for the analysis presented here. Steady-state behavior was simulated for various evaporator heat loads and mass of charge. Figure 9 illustrates the variation of evaporator temperature (T_1) with heat load in a CPL. The evaporator temperature of a CPL, with 135 g of charge, is nearly constant and the loop deprimes at about 440 W due to insufficient length of condenser (inadequately subcooled liquid at the inlet of the evaporator [7]). The system is in variable conductance mode because T_1 is nearly constant [1]. This is attributed to displacement of the liquid from the condenser to the two-phase reservoir, thereby increasing heat dissipating area ($\propto L_{condensation}$) in the condenser. This is evident in Fig. 10, in which the length of condensation and volume fraction of liquid in the reservoir (β) increases with Q_{load}. The steep P–T curve ($dP/dT|_{sat} \sim 3 \times 10^4$) at the operating temperatures, for ammonia, is also the cause for small rise in T_1 (variable conductance) with heat load and for T_1 being almost equal to the reservoir temperature (T_r) in a CPL. The two-phase reservoir controls the evaporator temperature through the pressure at state point 7 in a CPL where the reservoir is plumbed. With increase in load on the evaporator, P_1 would increase to overcome pressure drops in the vapor line, condenser, and liquid line (up to point 7), thus

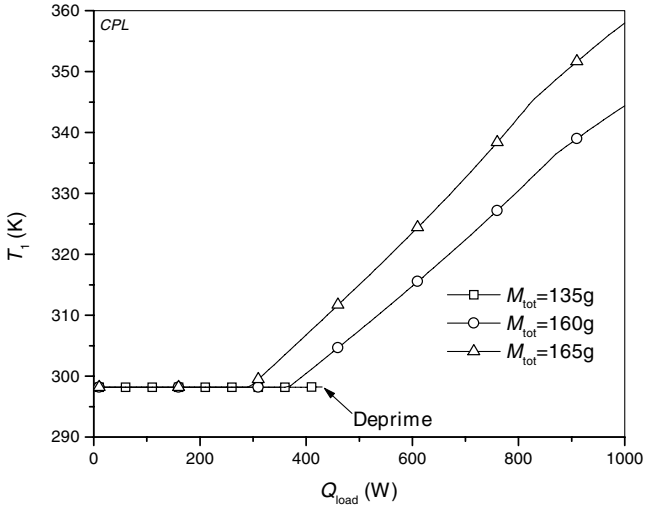

Fig. 9 Effect of mass of charge on variation of T_1 with Q_{load} in a CPL.

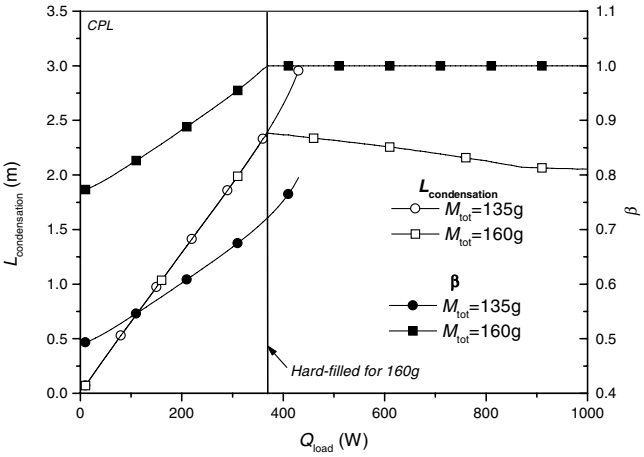

Fig. 10 Effect of mass of charge on $L_{condensation}$ and β in a CPL.

ensuring $P_7 = P_{7r}$. As the slope of the P–T curve for ammonia is large ($\sim 3 \times 10^4$), the change in T_1 is extremely small despite an increase in P_1–P_7 with heat load. If the reservoir temperature is increased, the temperature of the evaporator will increase and the system would deprime at a higher load (for reasons of limited condenser length).

In a CPL with 160 g charge, T_1 increases steeply for heat loads higher than 380 W (Fig. 9) indicating constant conductance operation due to hard-filling of the reservoir (Fig. 10). When the condenser gets hard-filled, the reservoir loses control on the loop. The pressure and temperature variation with heat load is controlled by boundary conditions like sink temperature, mass of charge, and fluid properties such as isothermal compressibility and volume expansivity. The inability to further increase the condensation length causes a steep rise in evaporator temperature with increase in heat load. If fluid in the hard-filled system were assumed to be incompressible, condensation length would not change with heat load, implying that the evaporator temperature would undergo a proportional increase in temperature with heat load. If liquid compressibility (reservoir), liquid expansivity (liquid line and subcooler), and vapor compressibility (vapor line and the condenser) are considered, the relationship between evaporator temperature and heat load in a hard-filled CPL is not exactly linear. The liquid expansivity in liquid line and subcooler, and vapor compressibility in vapor line and condenser causes the condensation length to reduce with increase in heat load (Fig. 10) in a hard-filled CPL. Table 3 gives the loads at which the CPL would deprime and the loads at which it would hard-fill.

In an LHP (Fig. 11) temperature variation with heat load is V-shaped. For small heat loads, the temperature of the evaporator reduces and temperature of the liquid leaving the condenser (T_3) is nearly constant. The liquid in the liquid line picks up (or loses) heat depending on the ambient conditions. In this study the ambient temperature is greater than the sink temperature. The rise in temperature along the liquid line can be explained (using LMTD) by $T_4 - T_3 = [\exp(U_{ll\text{-}\infty} A/\dot{m} C_p) - 1](T_\infty - T_3)$. Because flow in liquid line is (in general) laminar, $U_{ll\text{-}\infty}$ is nearly constant and $\dot{m}$

Table 3 Summary of characteristic heat loads in a CPL and LHP for different mass of charge in the system

M_{tot}	CPL		LHP	
	$Q_{deprime}$	Q_{hf}	Q_{open}	Q_{hf}
135 g	440 W	[b]	450 W	1100 W
145 g	440 W	[b]	450 W	650 W
155 g	[a]	420 W	[c]	330 W
160 g	[a]	370 W	[c]	220 W
165 g	[a]	300 W	[c]	180 W

[a]CPL does not deprime due to limited condenser length as it hard-fills before the condenser is fully used.
[b]CPL deprimes before it gets hard-filled, due to limited length of condenser.
[c]LHP hard-fills before condenser can open.

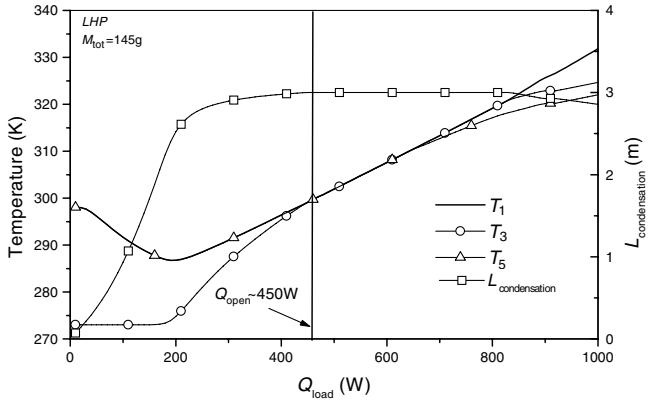

Fig. 11 Variation of T_1, T_3, T_5, and $L_{condensation}$ with Q_{load} in an LHP for $M_{tot} = 145$ g.

increases with heat load, the rise in temperature would be higher for smaller loads than at higher heat loads. Hence with increase in heat load the liquid line exit temperature reduces, which in turn reduces the core and the reservoir temperature, resulting in lower evaporator temperature. The subcooling in the condenser, $\dot{m}C_p(T_{2\text{cond}} - T_3)$, increases with increase in heat load, whereas T_3 is nearly constant. After a certain heat load, T_3 increases because of reduced subcooling length in the condenser. The load corresponding to *maximum* subcooling, has *minimum* evaporator temperature, further increase in heat load results in higher evaporator temperature.

After a certain load (Q_{open}), the temperature of evaporator increases linearly with heat load. This happens because the condenser has fully opened and there is some vapor in the fluid leaving the condenser, which is evident from Fig. 12, in which exit quality (x_3) increases at about 450 W ($Q_{\text{open}} \sim 450$ W). For heat loads greater than Q_{open}, the temperature of the evaporator increases linearly as the length available to reject heat is almost constant. This is when the LHP is said to have moved into constant conductance mode [3]. It is also observed in Fig. 12 that for a certain heat load greater Q_{open}, vapor enters the core. In spite of vapor entering the core, an LHP does not deprime [3,17]. The latent heat associated with the vapor leaving liquid line ($\dot{m}x_4h_{\text{fg4}}$) is lost to the ambient in the CC.

The core in an LHP is at saturation temperature corresponding to pressure in the core. The temperature difference across the wick could be related to the pressure drop in the loop by the Clausius–Clapeyron relation $T_1 - T_5 \sim (\Delta P_{\text{tot}} - \Delta P_w)/(\text{d}P/\text{d}T)_{\text{sat}}$. The temperature difference across the wick is very small due to the steep P–T curve of ammonia (at operating temperature) and small pressure drops in the loop. As a result, leak to the core of the evaporator (Q_{Lc}) and leak on the outer surface of the wick (Q_{Lo}) are also small as seen in Fig. 13.

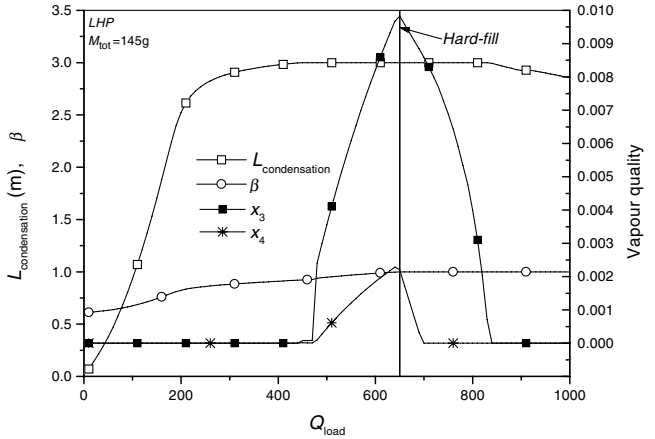

Fig. 12 Variation of $L_{condensation}$, β, x_3, and x_4 with Q_{load} for $M_{tot} = 145$ g.

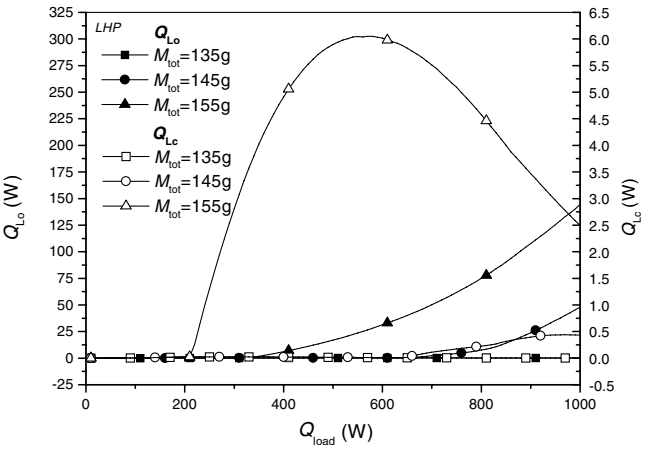

Fig. 13 Effect of mass of charge on heat leak on outer and inner surface of the wick in an LHP.

Unlike LHPs, CPLs have significant heat leaks on the outer surface of the wick and to the core (Fig. 14). This is attributed to the subcooled liquid in the core, which results in large temperature differences across the wick. Figure 15 shows variation of temperature with the heat load at different locations in a CPL. The leak to the core initially increases, but after a certain heat load it reduces. The reason is a rise in T_3 and reduction in γ [Eq. (10)] due to increased $\dot{m}$. In a CPL with 160 g charge the leak to core, after hard-filling at 380 W, increases due to an increase in temperature drop across the wick. Q_{Lc} reduces after certain heat load due to a large drop in γ with increased mass flow rate. Q_{Lo} monotonically increases with heat load in both variable and constant conductance modes.

Figure 16 illustrates the variation in β with heat load in an LHP. With increase in heat load, more fluid is injected into the reservoir due to an increase in condensation length. When the heat loads are greater than Q_{hf}, the reservoir (or CC) is full of liquid. Figure 16 shows that for $M_{\text{tot}} = 145$ g, β is unity for loads greater than 650 W. The core of a hard-filled LHP is *subcooled* and the temperature difference across the wick increases as seen in Fig. 11. When the LHP ($M_{\text{tot}} = 145$ g) is hard-filled (Fig. 12), the condenser is already open and vapor enters the core. After the CC is hard-filled, the vapor quality both at condenser exit and the liquid line exit reduces sharply. This is attributed to a steep rise in Q_{Lo} due to a larger temperature difference across the wick. For large heat loads ($>Q_{\text{hf}}$), the vapor completely condenses in the liquid line due to the large temperature difference with the ambient. As the load on the evaporator is increased further, the vapor completely condenses in the condenser and the condensation length starts reducing due to increase in evaporator temperature, compressibility of vapor in vapor line (and condenser) and expansivity of liquid in liquid line and CC. Once the

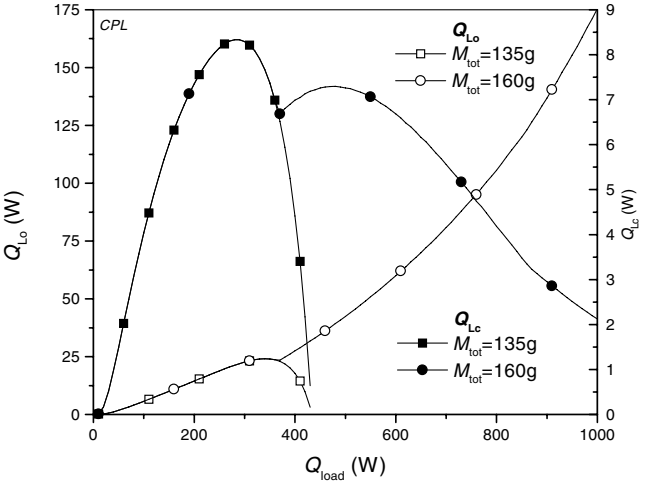

Fig. 14 Effect of mass of charge on heat leak on outer and inner surface of the wick in a CPL.

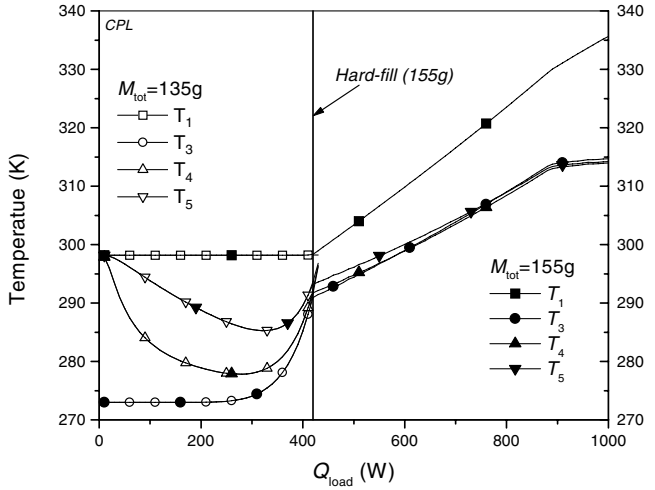

Fig. 15 Effect of mass of charge on various temperatures in a CPL.

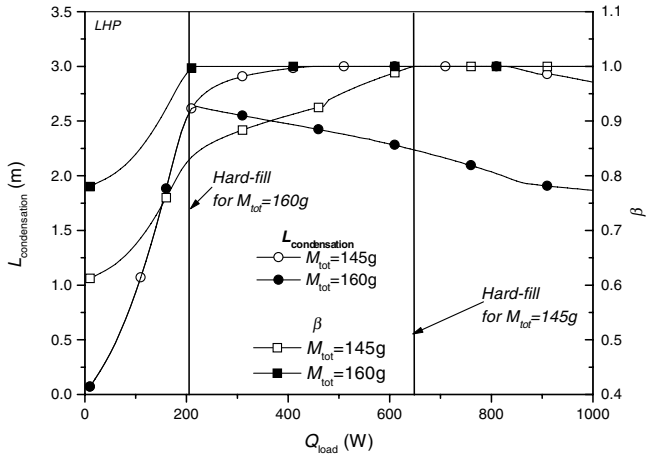

Fig. 16 Effect of mass of charge on variation of $L_{condensation}$ and β in an LHP.

liquid completely condenses in the condenser, subcooling increases in the condenser, and therefore T_3 separates from the evaporator temperature (Fig. 11).

The mass of charge affects the load at which hard-filling occurs (Q_{hf}). For a given system and boundary condition, Q_{hf} reduces with an increase in mass of charge. Figure 17 shows variation of evaporator temperature for different masses of charge in an LHP. With an increase in mass of charge, the LHP hard-fills at lower loads. The system with 135 g charge does not hard-fill even at 1000 W (hard-fills at about 1100 W) and the condenser fully opens up at 450 W. A system with 145 g of ammonia hard-fills at about 650 W; however, a significant rise in T_1 does not occur until the two-phase front withdraws from the liquid line and is limited to the condenser; this occurs at about 800 W. The steep rise in T_1 for heat loads beyond 800 W is attributed to reduction in two-phase heat transfer area as a result of reduction in the length of condensation, which is due to the liquid expansion (liquid line and CC) and vapor compression (condenser and vapor line). Table 3 gives the loads at which the LHP condenser opens and the hard-fills. For 155 g mass of charge the hard-fill occurs at about 330 W, and a steep rise in temperature of the evaporator occurs at the onset of hard-fill. CC of the LHP, with 155 g charge, hard-fills before condenser fully opens, provided the system has not hard-filled before the condenser opens. It should be noted here that Q_{open} is independent of mass of charge. A steep rise in temperature is attributed to the inability to increase length of condensation due to liquid expansivity effects . For an LHP with 155 g charge, T_1 separates from the non-hard-filled evaporator temperature curve as seen in Fig. 17. The separation of evaporator temperature, when hard-filled, for 160 g and 165 g masses of charge occurs at lower loads. It may be noted that for 165 g mass of charge,

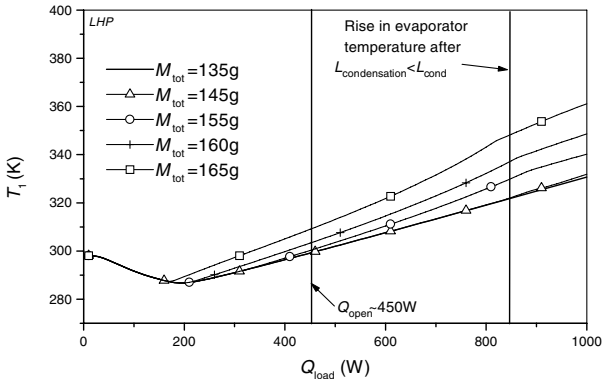

Fig. 17 Effect of mass of charge on evaporator temperatures in an LHP.

the evaporator temperature starts increasing even before the minimum evaporator temperature (287 K for an LHP with 135 g), is reached. This is similar to the case described by Maidanik [4] where an increase in evaporator temperature with heat load (after initial drop in T_1) is attributed to hard-filling of the compensation chamber.

V. Conclusions

In this study a mathematical model is developed to predict thermal and hydraulic performance of a CPL and an LHP including the effects of hard-filled reservoir or CC. The constant conductance mode of operation in the CPL occurred when the reservoir hard-filled. In the LHP, constant conductance occurred either by the condenser being fully used or by the CC getting hard-filled. In a CPL, the core is always subcooled, whereas in an LHP the core is subcooled only when the reservoir hard-fills. Both in the CPL and LHP it was observed that after hard-fill, the heat leaks increase significantly and hence the mass flow rate must be determined from an energy balance on the outer surface of the wick. The temperature difference across the wick also increased with heat load when either the CPL or LHP is hard-filled. The mass of charge in a CPL or an LHP influences the heat load at which hard-filling occurs. Further, after getting hard-filled, the length of condensation reduces with an increase in heat load due to expansivity of the liquid and compressibility of the vapor.

Acknowledgments

This work was carried out at ISRO Satellite Centre. The authors are grateful to D. R. Bhandari, R. A. Katti, P. P. Gupta, K. Badari Narayana, and D. Chakraborty (from ISRO Satellite Centre) for encouragement and suggestions.

References

[1] Ku, J., "Thermodynamic Aspects of Capillary Pumped Loop Operation," AIAA Paper 94-2059, 1994.
[2] Ku, J., "Recent Advances in Capillary Pumped Loop Technology," AIAA Paper 97-3780, 1997.
[3] Ku, J., "Operating Characteristics of Loop Heat Pipes," SAE Paper 1999-01-2007, 1999.
[4] Maidanik, Y. F., "Loop Heat Pipes," *Applied Thermal Engineering*, Vol. 25, April 2005, pp. 635–657.
[5] Pastukhov, V. G., Maidanik, Y. F., and Fershtater, Y. G., "Adaption of Loop Heat Pipes to Zero-G Conditions," *Proceedings of the Sixth European Symposium on Space Environmental Control Systems*, ESA SP-400, European Space Agency, Noordwijk, The Netherlands, 1997, pp. 385–391.
[6] Nikitkin, M., and Cullimore, B., "CPL and LHP Technologies: What are the Differences, What are the Similarities," SAE Paper 981587, 1998.
[7] Maidanik, Y. F., Fershtater, Y. G., and Pastukhov, V. G., "Design and Investigation of a Capillary Pumped Loop for Advanced Thermal Control Systems of Space Vehicles," SAE Paper 951509, 1995.
[8] Stenger, F. J., "Experimental Feasibility Study of Water-Filled-Capillary-Pumped Heat-Transfer Loops," NASA Lewis Research Center Tech. Rep. NASA TM-X-1310, Cleveland, OH, 1966.

[9] Maidanik, Y. F., Vershinin, S., Kholdov, V., and Dolgirev, J., "Heat Transfer Apparatus," U.S. Patent No. 4515209, 1985.
[10] Muraoka, I., Ramos, F. M., and Vlassov, V. V., "Experimental and Theoretical Investigation of a Capillary Pumped Loop with a Porous Element in the Condenser," *International Communications in Heat and Mass Transfer*, Vol. 25, No. 8, 1998, pp. 1085–1094.
[11] Muraoka, I., Ramos, F. M., and Vlassov, V. V., "Analysis of Operational Characteristics and Limits of a Loop Heat Pipe with Porous Element in Condenser," *International Journal of Heat and Mass Transfer*, Vol. 44, No. 12, June 2001, pp. 2287–2297.
[12] Kiper, A., Feric, G., Anjum, M., and Swanson, T., "Transient Analysis of a Capillary Pumped Loop Heat Pipe," AIAA Paper 90-1685, 1990.
[13] Wulz, H. G., and Embacher, E., "Capillary Pumped Loops for Space Application. Experimental and Theoretical Studies on Performance of Capillary Evaporator," AIAA Paper 90-1739, 1990.
[14] Pouzet, E., Joly, J. L., Platel, V., Grandpeix, J. Y., and Butto, C., "Dynamic Response of Capillary Pumped Loop Subjected to Various Heat Load Transients," *International Journal of Heat and Mass Transfer*, Vol. 47, Dec. 2004, pp. 2293–2316.
[15] Schweickart, R. B., and Neiswanger, L., "Verification of an Analytical Modeller for Capillary Pump Loop Thermal Control System," AIAA Paper 87-1630, 1987.
[16] Dickey, J. T., and Peterson, G. P., "Experimental and Numerical Investigation of a Capillary Pumped Loop," *Journal of Thermophysics and Heat Transfer*, Vol. 8, No. 3, 1994, pp. 602–607.
[17] Parker, M. L., "Modeling of Loop Heat Pipes with Applications to Spacecraft Thermal Control," Ph.D. Dissertation, Dept. of Mechanical Engineering and Applied Mechanics, Univ. of Pennsylvania, Philadelphia, 2000.
[18] Kaya, T., and Hoang, T. T., "Mathematical Modelling of Loop Heat Pipes and Experimental Validation," *Journal of Thermophysics and Heat Transfer*, Vol. 13, No. 3, 1999, pp. 314–320.
[19] Chuang, P.-Y. A., "An Improved Steady-State Model of Loop Heat Pipes Based on Experimental and Theoretical Analysis," Ph.D. Dissertation, Dept. of Mechanical and Nuclear Engineering, The Pennsylvania State University, University Park, PA, 2003.
[20] Faghri, A., *Heat Pipe Science and Technology*, Taylor & Francis, Washington, DC, 1995, pp. 578–620.
[21] Bonnefoy, M., Ochterbeck, J. M., Drolen, B. L., and Nikitkin, M. N., "Effective Thermal Conductivity of Saturated Sintered Nickel Loop Heat Pipe Wicks," AIAA Paper 2004-2571, 2004.
[22] Maidanik, Y., Fershtater, Y., Pastukhov, V. G., and Chernysheva, M., "Experimental and Theoretical Investigation of Startup Regimes of Two-Phase Capillary Pumped Loops," SAE Paper 932305, 1993.
[23] Peterson, G. P., *Introduction to Heat Pipes*, John Wiley & Sons, New York, 1994.
[24] Jasvanth, V. S., Ambirajan, A., Adoni, A. A., Kumar, D., Gupta, P. P., Bhandari, D. R., and Srinivasan, K., "Preliminary Experiments with Capillary Pumped Loop with a Flat Plate Evaporator," HMT Paper 2006-C164, 2006.
[25] Rohsenow, W. M., Hartnett, J. P., and Cho, Y. I. (eds.), *Handbook of Heat Transfer*, McGraw–Hill, New York, 1998.
[26] Chapra, S. C., and Canale, R. P., *Numerical Methods for Engineers*, McGraw–Hill, New York, 2002, pp. 154–157 and 681–725.
[27] Carey, V. P., *Liquid-Vapour Phase Change Phenomena*, Taylor & Francis, Washington, DC, 1992, pp. 399–482.
[28] Hajal, J. E., Thome, J. R., and Cavallini, A., "Condensation in Horizontal Tubes, Part 1: Two-Phase Flow Pattern Map," *International Journal of Heat and Mass Transfer*, Vol. 46, No. 18, Aug. 2003, pp. 3349–3363.
[29] Thome, J. R., Hajal, J. E., and Cavallini, A., "Condensation in Horizontal Tubes, Part 2: New Heat Transfer Model Based on Flow Regimes," *International Journal of Heat and Mass Transfer*, Vol. 46, No. 18, Aug. 2003, pp. 3365–3387.
[30] Tomlinson, B. J., "Steady State Analysis of the USAF Philips Laboratory Capillary Pumped Loop Testbed," SAE Paper 97032, 1997.
[31] Furukawa, M., "Model-Based Method of Theoretical Design Analysis of a Loop Heat Pipe," *Journal of Thermophysics and Heat Transfer*, Vol. 20, No. 1, 2006, pp. 111–121.